Journal of Mechanics in Medicine and Biology
Vol. 15, No. 3 (2015) 1550029 (13 pages)

DOI: 10.1142/S0219519415500293

World Scientific
www.worldscientific.com

MECHANICAL STRESS IN ABDOMINAL AORTIC ANEURYSMS USING ARTIFICIAL NEURAL NETWORKS

EDUARDO SOUDAH*,§, JOSÉ F. RODRÍGUEZ† and ROBERTO LÓPEZ‡

*International Center for Numerical Methods in Engineering (CIMNE)
Biomedical Engineering Depart., Technical University of Catalonia (UPC)
08034 Barcelona, Spain

†Aragón Institute of Engineering Research
Group of Applied Mechanics and Bioengineering
(I3A), University of Zaragoza, 50018 Zaragoza, Spain

‡Research and Development Department, Intelnics.
Carretera de Madrid 13, 37900 Santa Marta de Tormes,
Salamanca, Spain
§esoudah@cimne.upc.edu

Received 2 August 2014
Revised 27 August 2014
Accepted 28 August 2014
Published 14 October 2014

Combination of numerical modeling and artificial intelligence (AI) in bioengineering processes are a promising pathway for the further development of bioengineering sciences. The objective of this work is to use Artificial Neural Networks (ANN) to reduce the long computational times needed in the analysis of shear stress in the Abdominal Aortic Aneurysm (AAA) by finite element methods (FEM). For that purpose two different neural networks are created. The first neural network (Mesh Neural Network, MNN) creates the aneurysm geometry in terms of four geometrical factors (asymmetry factor, aneurism diameter, aneurism thickness, aneurism length). The second neural network (Tension Neural Network, TNN) combines the results of the first neural network with the arterial pressure (new factor) to obtain the maximum stress distribution (output variable) in the aneurysm wall. The use of FEM for the analysis and design of bioengineering processes often requires high computational costs, but if this technique is combined with artificial intelligence, such as neural networks, the simulation time is significantly reduced. The shear stress obtained by the artificial neural models developed in this work achieved 95% of accuracy respect to the wall stress obtained by the FEM. On the other hand, the computational time is significantly reduced compared to the FEM.

Keywords: Artificial neural network; AAA; real time.

1. Introduction

About 90% of Abdominal Aorta Aneurysms (AAA) are located below the level of the renal arteries. This pathology is known as infrarenal aneurysm, and involves the

§Corresponding author.

enlargement of the aorta in the inferior thoracic area. It takes a fusiform shape and might extend into the iliac arteries. The mortality by infrarenal aneurysms is high (15% for ruptured aneurysms), and the current standard of determining rupture risk is based on the maximum diameter. One of these AAA rupture criteria are based on the aortic size (diameter) and the rate of growth.[1] This criterion is based on Laplace law for hollow cylinders, which establishes that maximum stress in the artery increases with the radius. Other authors[2–5] based on the AAA shape as its asymmetry or tortuosity have proposed different criteria for the AAA collapsibility, if the AAA diameter is higher than 5.5 cm the AAA may rupture[2]; if the asymmetry index factor, $\beta < 0.4$ the AAA rupture risk is high[3]; if the deformation diameter ratio is $\chi > 3.3$ the AAA might collapse[4]; if the saccular index is < 0.6 the rupture risk is high.[5] But depending on the index that is analyzed the surgical criteria is different. All above studies suggest that not only size but also the shape of the aneurysm appears to be important factors in determining the risk of rupture of a given aneurysm. Therefore, alternative approach of AAA rupture assessment and other biomechanical variables are needed. The majority of these new approaches involve the numerical analysis using finite element methods (FEM) to determine new biomechanical variables inside the AAA.[6–9]

In this line, during the last period, some authors suggest that peak wall stress correlated with the AAA geometrical factors is the more reliable parameter for the assessment of the rupture risk of aortic aneurysms.[10–14] Filinger *et al.*[14] found that peak wall stress in aneurysms has a higher sensitivity (patients that went under rupture) and specificity (patients which did not undergo rupture) than maximum diameter. These findings appear to be supported by the results obtained by Ref. 8, who analyzed 27 aneurysms (15 nonruptured and 12 ruptured) using the finite element method. In their study, the peak wall stress in the ruptured aneurysms was found to be about 60% higher than for the nonruptured aneurysms. Also, the rupture location matched the area of maximum stress.[15,16] However, the use of finite element methods for the analysis of AAA often requires long computational times. For that reason, the purpose of this work is to develop an artificial neural network to compute the peak stress in real time over the aneurysm wall. To achieve our goal we combine, in a multidisciplinary framework, numerical analysis (finite element) and artificial neural networks (ANN) for the simulation of an aneurysms rupture. To study the peak stress over the AAA wall, a hyperplastic isotropic model without considering the fiber orientation has been implemented using FEM. Based on this arterial model, 243 idealized AAA were generated and simulated. Using the results obtained using the finite element technique, two different neural networks were developed and trained, a Mesh Neural Network (MNN) and a Tension Neural Network (TNN). The first one (MNN) creates an aneurysm mesh in terms of four geometrical factors (asymmetry factor, aneurysm diameter, aneurysm thickness, aneurysm length). And the second neural network (TNN) is coupled with the MNN to calculate the peak wall shear stress on every node of that mesh for a given arterial pressure.

2. Geometrical and Material Model

The shape of an aneurysm can be defined by a "parabolic-exponential shape" function proposed by Elger *et al.*,[4] see Fig. 1.

The mathematical function of this geometry is given by:

$$R(z) = R_a + \left(R_{\text{an}} - R_a - c_3 \frac{Z^2}{R_a^2}\right) \cdot e^{-(c_1 \cdot |\frac{Z}{R_a}|^{c_2})}, \tag{1}$$

where R_a is the radius of the un-diseased artery, R_{an} is the maximum radius of the aneurysm. On the other hand, c_1 is a constant to be taken as 5.0, c_2 and c_3 are dimensionless geometrical parameters depending on the geometry of the aneurysm according to:

$$c_2 = \frac{4.605}{(0.5 L_{\text{an}} R_a)^{c_1}}, \tag{2}$$

$$c_3 = \frac{R_{\text{an}} - R_a}{R_a \cdot (\frac{0.8 L_{\text{an}}}{R_a})^2}, \tag{3}$$

where L_{an} defines the length of the aneurysm and e is the eccentricity between the aneurysm and the nonpathological arterial vessel.

In order to study the effect of the AAA geometry on the distribution of the wall stresses we introduce three (dimensionless) geometrical parameters:

$$F_R = \frac{R_{\text{an}}}{R_a}, \tag{4a}$$

$$F_L = \frac{L_{\text{an}}}{R_{\text{an}}}, \tag{4b}$$

$$F_E = \frac{e}{R_a \cdot (F_R - 1)}, \tag{4c}$$

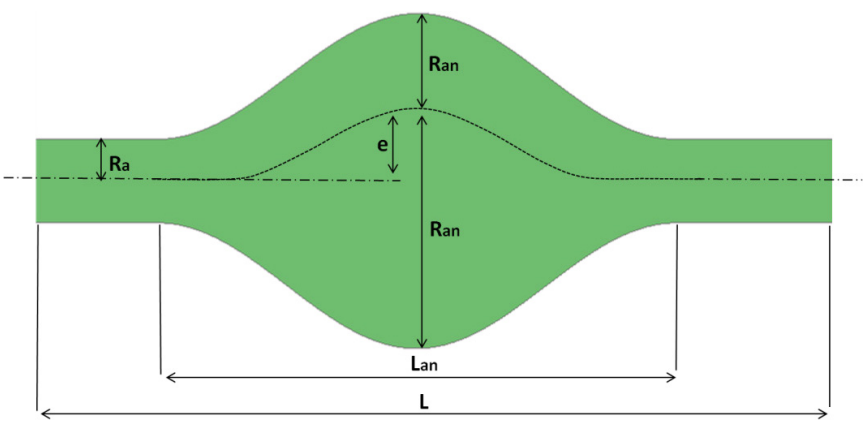

Fig. 1. Idealized geometric model of an AAA with "parabolic-exponential shape".

Table 1. Range of the values F_R, F_L, F_T and β.

Parameter	Description	Range
B	Asymmetry factor	0–1
F_R	Radius factor	2–2.75
F_L	Length factor	1.5–3
F_T	Thickness factor	0.6–1

where $F_R \geq 1$ defines the ratio between the maximum AAA radius and the undiseased arterial radius, F_L defines the ratio between the length of the aneurysm and the maximum AAA radius, and $F_E \in [0, 1]$ is a measure of the aneurismal eccentricity, with e as indicated in Fig. 1 (e is the actual eccentricity between the center of the nonpathological arterial vessel and the center of the section where the maximum aneurismal diameter is located).

The extreme cases are symmetric $F_E = 0$ (with $e = 0$), intermediate eccentric $F_E = 0.5$ and extreme eccentric $F_E = 1$ (with $e = R_{\text{an}} - R_a$). The range of the values F_R and F_L given in Table 1 is in good agreement with values used in previous parametric studies[2] as well as with clinical investigations [4, 10, 11, 19], where F_R ranges from 2.0 to 2.75 and F_L from 1.5 to 3.0. The wall thickness is assumed to be uniform, with 1.5 mm,[7] and the arterial radius is considered to be $R_a = 10.1$ mm. The constant wall thickness assumption has been used in a number of previous studies.[2,6,7,15] In this work random combinations of these parameters were used to create different AAA geometries using GiD.[17] All parametric solid models were meshed with 16896 hexahedral incompressible elements and 25536 nodes using GiD.[17] Figure 2 illustrates six different AAA configurations for different parameters.

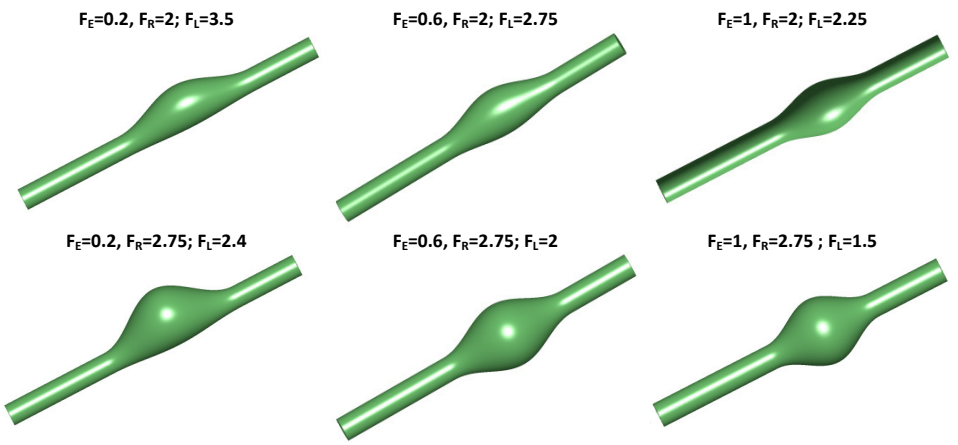

Fig. 2. Geometric models of AAA for three values of aneurismal eccentricity (0.2, 0.6, 1) and for the extreme values for F_R (2–2.75) and F_L (1.5–3).

On the other hand, experimental studies of mechanical properties of the AAA show that high peak wall stress can provoke damage over the arterial wall, and its value can be used as predictor of arterial failure.[18] Therefore, the material model should be able to accurately draw a relation between geometric factors and peak wall shear stress.[19] Based on the knowledge that the AAA wall is incompressible and most likely undergoes large deformations,[18] we can employ the multiplicative decomposition of the deformation gradient F into a volumetric part $J^{-1/3}I$, and an isochoric part $\bar{F}$, with the volume ratio $J = \det F > 0$ and $\det \bar{F} = 1$. By using an additive decomposition of W, we can write[20]:

$$\Psi(C) = U(J) + \bar{\Psi}(\bar{I}_1 \bar{I}_2 \bar{I}_4, \ldots, \bar{I}_8), \tag{5}$$

where $\bar{C} = \overline{F^T} \cdot \bar{F}$ is the right Cauchy Green tensor, and the volumetric elastic response U and the isochoric elastic response Ψ of the material are given scalar-valued objective functions of J and the invariants $\bar{I}_1, \bar{I}_2, \bar{I}_4, \ldots, \bar{I}_8$, respectively.

On assumption that the behavior of the AAA wall is hyperplastic isotropic, and without considering the fiber orientation, the strain energy density W for this material can be written as:

$$W = U(J) + c_{10}(\bar{I}_1 - 3) + c_{20}(\bar{I}_1 - 3)^2, \tag{6}$$

where I_1 is the first invariant, $\bar{I}_1 = \mathrm{tr}(\bar{C})$, of the deviatoric right Cauchy Green tensor $\bar{C}$ is the deviatoric deformation gradient tensor and C_{10} and C_{20} are the model parameters indicative of the mechanical properties of the AAA wall ($C_{10} = 174\,\mathrm{kPa}$, $C_{20} = 1880\,\mathrm{kPa}$).[7]

A range of pressure between 12.3–15.7 kPa was applied to simulate the end systolic conditions, since this pressure represents the stage of the cardiac cycle in which the AAA experiences the largest wall stress. The longitudinal constraining at the proximal and distal parts of the aneurysm due to the renal and iliac arteries was simulated by constraining the displacements to be zero at both ends.[7,15]

After developing the geometrical and computational model, 243 AAA were simulated as a random combination of the geometrical factor (see Table 1) and the internal pressure (12.3–15.7 kPa).

3. Artificial Neural Networks

During the last few years, ANN have found a wide range of applications. One of the most popular learning tasks here is function regression, also called data modeling. The function regression problem can be regarded as the problem of approximating a function from data. These applications always involve a data set, a neural network, a performance functional and a training strategy. The learning problem is then formulated as to find a neural network which optimizes a performance functional by means of a training strategy.[21]

The data set contains the information for creating the model. It comprises a matrix in which columns represent variables and rows instances. Variables in a data set can be of two types: The inputs will be the independent variables, and the targets will be the dependent variables. On the other hand, instances can be: Training instances, which are used to construct the model; generalization instances, which are used for selecting the complexity and testing instances, which are used to validate the functioning of the model.

The neural network defines a function which represents the model. The neural network used here is based on a multilayer perceptron (MLP) with a sigmoid hidden layer and a linear output layer, which is a class of universal approximator.[21] That neural network is also extended with scaling and unscaling layers.

The performance functional plays an important role in the use of neural networks, since it defines the task that the neural network is required to accomplish. The mean squared error is the performance functional used in this work. It measures the difference between the outputs from the neural network and the targets in the data set.[23] The procedure used to carry out the learning process is called training strategy. The training strategy is applied to the neural network in order to obtain the best possible performance. The type of training is determined by the way in which the adjustment of the parameters in the neural network takes place. The quasi-Newton method is the training strategy used here.[23]

In this work, we have designed, trained and validated two artificial neural networks: a MNN to create the computational mesh of the AAA based on the geometrical factors, and a TNN to compute the peak wall shear stress over the AAA wall. The open neural networks library OpenNN[24] has been used for that purpose.

3.1. *Mesh neural networks*

The aim of the MNNs is to create the computational mesh of the AAA in a precise and fast mode. Here, a vector of neural networks with size the number of nodes in the mesh will be created. The number of nodes for all the computational mesh is the same, 25,536 nodes. The inputs to the MNN are the aneurism geometry factors (F_L, F_R, F_T) and the asymmetric factor (β) defined previously. The outputs from the MNN are the corresponding node coordinates (X, Y and Z). While the numbers of inputs and outputs are constrained by the problem, the complexity of the model, defined by the number of hidden neurons in the network, is a design variable. A model order selection analysis showed that 12 neurons in the hidden layer is the optimal architecture for this problem. Figure 3 is a graphical representation of this network architecture.

Defined the input–output variables of the MNN, a data set must be generated for training. In this work an iso-topological hexahedral mesh is considered (Fig. 4). That means that the number and arrangement of nodes and elements is always the same, only the node coordinates can change. All parametric solid models were meshed using the commercial software GiD with 16,896 hexahedral incompressible

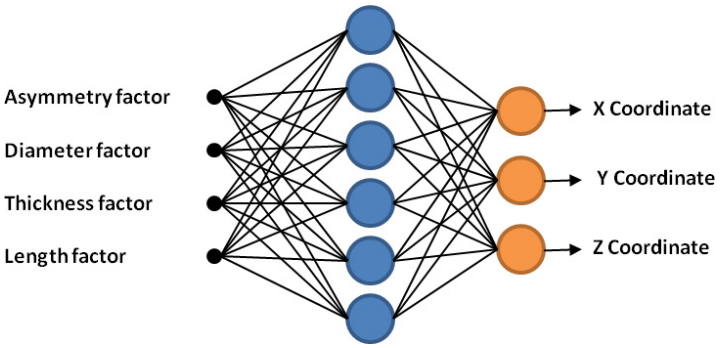

Fig. 3. Neural network architecture for the mesh multilayer perceptron, with 4 inputs, 12 neurons in the hidden layer and 3 output neurons.

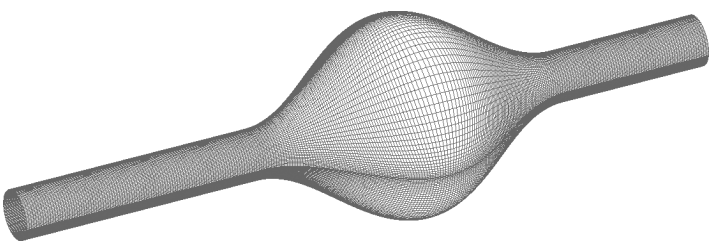

Fig. 4. Hexahedral finite element mesh used for the analysis.

elements and 25,536 nodes. In this way, a vector of data sets has been created, where the number of elements in the vector is equal to the number of nodes, that is, 25,536. Therefore, each element of the MNN will predict the coordinates of the corresponding node.

The number of samples in the data set is a design variable in the problem. In this work, we have used an input target data set with 243 samples for training. The ranges of the input variables are shown Table 1.

Figure 5 shows two examples of the MNN. Table 2 illustrates the data set for a given node.

As nodes positions are not smoothly distributed, the mesh obtained by the MNN gives us noisy results. However, results for meshes already seen by the neural network are not that noisy, and therefore we can use a nearest neighbor approach to solve this problem.

3.2. *Tension neural network*

The aim of the TNN is to calculate the peak wall shear stress over each node of the computational mesh generated by the MNN in a precise and fast mode. The first step for creating the TNN was to choose the network architecture to represent the main shear stress components T_x, T_y, T_z on the mesh generated previously by the

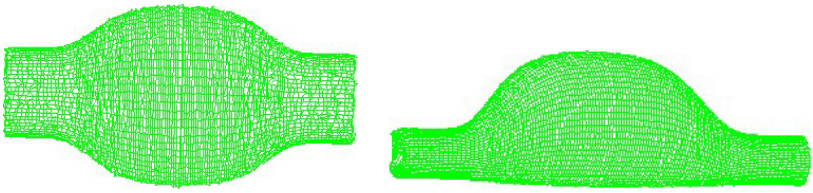

(a) (b)

Fig. 5. MNN for $\beta = 0$, $F_R = 2$, $F_T = 0.6$ and $F_L = 1.5$ (a), neural network mesh for $\beta = 1$, $F_R = 2.75$, $F_T = 1$ and $F_L = 2.5$ (b).

MNN. In this way, a vector of neural networks has been created, where the number of elements in the vector is equal to the number of nodes (25,536 in this case).

As before, a MLP with a sigmoid hidden layer and a linear output layer was used. The number of hidden neurons used in the TNN was 10, as it proved good generalization capabilities in this problem. The inputs to the neural network must characterize the X, Y, Z coordinate obtained in the MNN plus the pressure on that artery (P). We include the arterial pressure as an input variable to the neural network (range of pressure between 12.3–15.7 kPa) as inlet conditions for the numerical simulations. The outputs from each neural network are the main shear stress components on the artery, main shear stress x (T_x), main shear stress y (T_y) and main shear stress z (T_z). Figure 6 is a graphical representation of that network architecture.

Defined the input–output variables of the TNN, the second step was to generate the input-target data set. As previously, we have used an input target data set with 243 samples for training. For each sample a numerical simulation was done in a dual-core 2.83 GHz CP, Microsoft Windows XP 32-bit PC with 4 GB-RAM, with a total computation time of approximately five hours. Each simulation provides the shear stress state for each node (T_x, T_y and T_z), and the number of elements in the vector is equal to the number of nodes, that is, 25,536. Each input-target data set will be used for training the TNN.

The number of input variables in the data set must be equal to the number of input variables in the neural network, that is, 4. Similarly, the number of target variables in the data set must be equal to the number of output variables in the

Table 2. Data set for the MNN, with 243 samples, 4 input variables and 3 target variables.

Input variables				Output variables		
β	F_R	F_T	F_L	X coordinate	Y coordinate	Z coordinate
0.0	2.0	0.6	1.5	10.198	0.000	−39.395
0.5	2.75	0.6	1.5	15.154	10.541	−54.169
...	...	...	...	...	...	...
1.0	2.75	1.0	2.5	26.687	25.142	1.255

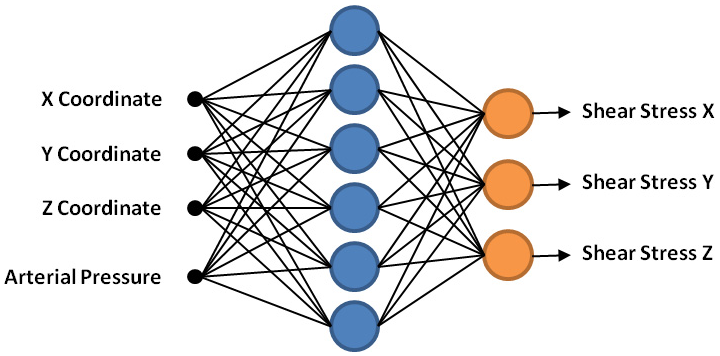

Fig. 6. Network architecture for the TNN.

neural network, that is, 3. Table 3 is a graphical representation of that input target data set.

The third step was to choose a suitable objective functional in order to formulate the function regression problem. Here we use the mean squared error between the outputs from the network and the targets in the data set. And the last step was to choose a training algorithm for solving the reduced function optimization problem. As before a quasi-Newton method with BGFS train direction and Brent optimal train rate is used.[23] The training algorithm is set to stop after 250 iterations. Once the TNN has been created it is ready for use. Figure 7 shows the results, main stresses, for three different cases based on aneurism geometry factors defined previously F_L, F_R, F_T, asymmetric factor (β) and an internal pressure (P).

4. Final ANN and Validation

Figure 8 shows the final neural network developed, where four dimensionless parametric factors: (1) AAA asymmetric factor, (2) AAA diameter factor, (3) AAA thickness factor and (4) AAA length factor are used together with hemodynamic arterial pressure factor to obtain the maximum peak stress over each node of the computational mesh.

Table 3. Data set for the MNN, with 243 samples, 4 input variables and 3 target variables.

Input variables				Output variables		
X coordinate	Y coordinate	Z coordinate	P	T_X	T_Y	T_Z
10.198	0.000	−39.395	12.3	10.198	0.000	−39.395
15.154	10.541	−54.169	12.3	15.154	10.541	−54.169
...	...	...		...	...	...
26.687	25.142	1.255	15.7	26.687	25.142	1.255

Parameters		Main Stresses
MNN	TNN	Main Tension T_x for:
β=0 F_L = 1.5 F_R=2 F_E=0.6	$[X]_i$ $[Y]_i$ $[Z]_i$ P=12.3 Pa	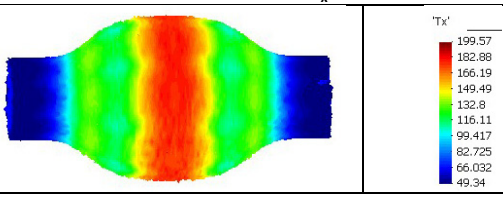
MNN	TNN	Main Tension T_y for:
β=0.5 F_L = 1.75 F_R=2.5 F_E=1.5	$[X]_i$ $[Y]_i$ $[Z]_i$ P=13.5 Pa	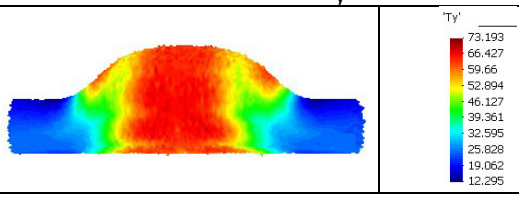
MNN	TNN	Main Tension T_z for:
β=1 F_L = 2.5 F_R=2.75 F_E=1	$[X]_i$ $[Y]_i$ $[Z]_i$ P=15.07 Pa	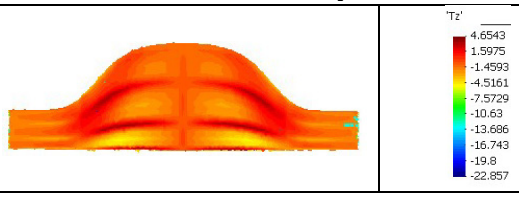

Fig. 7. Main shear stress components T_x, T_y and T_z calculations using the TNN for 3 different cases. $[X]$, $[Y]$, $[Z]$ represent the i-node coordiantes created using the aneurism factor (F_L, F_R, and F_T and the asymmetric factor (β)).

To validate the final network developed, the aneurismal principal stresses predicted by the AAA were compared with results obtained from finite element calculations for an aneurismal internal pressure for 27 random cases. The prediction of the error for each principal stress has been quantified according to:

$$\mathbf{error} = \frac{|\mathbf{S} - \mathbf{S}^{\mathbf{TNN}}|_\infty}{|\mathbf{S}|_\infty},$$

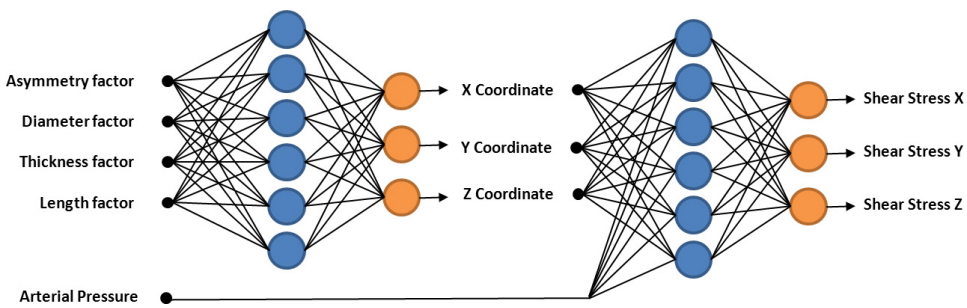

Fig. 8. Final artificial neural network developed. Input variables (F_R, F_L, F_T, β, pressure) and output variables (shear stress X, shear stress Y, shear stress Z).

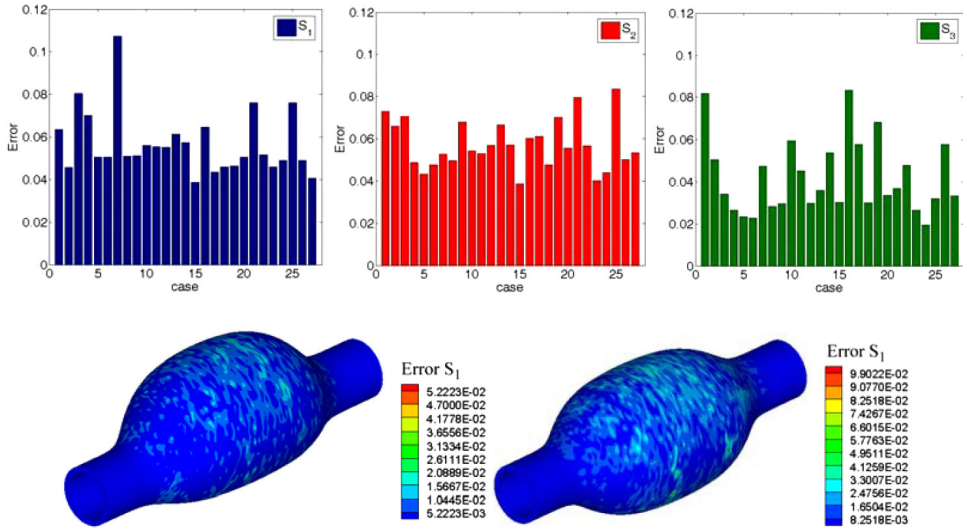

Fig. 9. Shown the error in the maximum principal stress for 27 cases analyzed (top). Shown the error S between the ANN against FEM for two different geometries (bottom).

where S is the vector of the principal stress at each node obtained using FE and S^{TNN} is the vector of principal stress at each node obtained by the TNN. According to Fig. 9, the results obtained in these 27 cases analyzed, the error for the principal stresses between the final network and the FE is negligible, less than 10%, and moreover the time is reduced in more than 95%.

5. Conclusions

The overall goal of this paper is to propose a comprehensive computational methodology based on structural analysis and ANN to predict the main stresses in the aneurysm wall in real time. A key feature of the proposed methodology is that the ANN are capable to reproduce the abdominal geometry and approximate the results of the FEM analysis up to a high degree of accuracy. In order to achieve the objective of this work, two different neural networks were created, a MNN to approximate the computational mesh and a TNN to approximate the shear stress components in the AAA. The main stresses obtained by the TNN compared with the FE are negligible as we have shown in Fig. 9. We recognize that the computational model used to simulate the AAA (hyperplastic isotropic and without considering the fiber orientation) is not the most accurate to reproduce the mechanical behavior of the wall. However the methodology suggested in this work could be used to predict the evolution or rupture of the AAA based only on geometrical factors and internal pressure in a real time. A full AAA structural analysis to obtain the main stresses over the wall requires 5 h in a desktop computer (aneurism model CAD, volume mesh generation and a structural analysis), whereas the framework proposed in this

work requires less than 2 min. The only parameters needed are the F_L, F_R, F_T, β and an internal pressure (P). Since this work was not based on patient-specific geometry, the geometrical parameters can be easily obtained using image processing techniques and pressure can be measured using a pressure cuff. Note that we have used a constant wall thickness, which is an assumption, the thickness distribution along the AAA changes.

To conclude, it is important to emphasize that computational modeling techniques combined with artificial intelligence procedures can provide an insight into the patient-specific conditions for AAA evolution or rupture in real time. Also, the methodology proposed allows to understanding the geometrical factors governing the maximum stresses in the aneurysm wall. Future studies, an improved material model (anisotropic model) will be developed, as well as, other geometrical factors as the tortuosity of the AAA. In addition, further studies are required to include the effect of the intraluminal thrombus.

References

1. Vorp DA, Biomechanics of abdominal aortic aneurysm, *J Biomech* **40**:1887–1902, 2007.
2. Vorp DA, Raghavan ML, Webster M, Mechanical wall stress in abdominal aortic aneurysm: Influence of diameter and asymmetry, *Eur J Vasc Surg* **27**(4):632–639, 1998.
3. Cappeller WA, Engelmann H, Blechschmidt S, Wild M, Lauterjung L, Possible objectification of a critical maximum diameter for elective surgery in abdominal aortic aneurysms based on one-and three-dimensional ratios, *J Cardiovasc Surg* **38**:623–628, 1997.
4. Elger DF, Blackketter RS, Budwig RS, Johansen KH, The influence of shape on the stresses in model abdominal aortic aneurysms, *J Biomech Eng* **118**:326–332, 1996.
5. Ouriel K, Green RM, Donayre C, Shortell CK, Elliott J, Deweese JA, An evaluation of new methods of expressing aortic aneurysm size: Relationship to rupture, *J Vasc Surg* **15**:12–20, 1992.
6. Venkatasubramaniam AK, Fagan MJ, Mehta T, Mylankal KJ, Ray B, Kuhan G, Chetter IC, McCollum PT, A comparative study of aortic wall stress using finite element analysis for ruptured and non-ruptured abdominal aortic aneurysms, *Eur J Vasc Surg* **28**(2):168–176, 2004.
7. Raghavan ML, Vorp DA, Toward a biomechanical tool to evaluate rupture potential of abdominal aortic aneurysm: Identification of a finite strain constitutive model and evaluation of its applicability, *J Biomech* **33**:475–482, 2000.
8. Gasser TC, Auer M, Labruto F, Swedenborg J, Roy J, Biomechanical rupture risk assessment of abdominal aortic aneurysms: Model complexity versus predictability of finite element simulations, *Eur J Vasc Endovasc* **40**:176–185, 2010.
9. Kleinstreuer C, Li Z, Analysis and computer program for rupture-risk prediction of abdominal aortic aneurysms, *Biomed. Eng. OnLine* **5**:19, 2006.
10. Soudah E, Ng EYK, Loong TH, Bordone M, Pua U, Narayanan S, CFD modelling of abdominal aortic aneurysm on hemodynamic loads using a realistic geometry with CT, *Comput Math Methods Med* **2013**, 2013, doi:10.1155/2013/472564.
11. Soudah E, Villalta G, Bordone M, Nieto F, Vilalta JA, Vaquero C, Hemodynamic on abdominal aortic aneurysm: Parametric study, Revista Int de Métodos Numéricos para Cálculo y Diseño en Ingeniería, Available at: http://dx.doi.org/10.1016/j.rimni.2014.02.003

12. Ouriel K, Green RM, Donayre C, Shortell CK, Elliott J, Deweese JA, An evaluation of new methods of expressing aortic aneurysm size: Relationship to rupture, *J Vasc Surg* **15**:12–20, 1992.
13. Georgakarakos E, Ioannou CV, Kamarianakis Y *et al.*, The role of geometric parameters in the prediction of abdominal aortic aneurysm wall stress, *Eur J Vasc Endovasc Surg* **39**:42:48, 2010.
14. Fillinger MF, Marra SP, Raghavan ML, Kennedy FE, Prediction of rupture risk in abdominal aortic aneurysm during observation: Wall stress versus diameter, *J Vasc Surg* **37**(4):724–732, 2003.
15. Inzoli F, Boschetti F, Zappa M, Longo T, Fumero R, Biomechanical factors in abdominal aortic aneurysm rupture, *Eur J Vasc Surg* **7**:667–674, 1993.
16. Vorp DA, Lee PC, Wang DHJ, Makaroun MS, Nemoto EM, Ogawa S *et al.* Association of intraluminal thrombus in abdominal aortic aneurysm with local hypoxia and wall weakening, *J Vasc Surg* **34**:291–299, 2001.
17. GiD — The personal pre and postprocessor, http://www.gidhome.com/ CIMNE.
18. Drangova M, Holdsworth D, Boyd CJ, Dunmore PJ, Roach MR, Fenster A, Elasticity and geometry measurements of vascular specimens using a high-resolution laboratory CT scanner, *Physiol Meas* **14**:277–290, 1993.
19. Rodríguez JF, Ruíz C, Doblaré M, Holzapfel GA, Mechanical stresses in abdominal aortic aneurysm: Influence of diameter, asymmetry and material anisotropy, *J Biomech Eng* **130**(2):021023, 2008.
20. Holzapfel GA, Gasser TC, Ogden RW, A new constitutive framework for arterial wall mechanics and a comparative study of material models, *J Elast* **61**:1–48, 2000.
21. Hornik K *et al.*, Multilayer feed forward networks are universal approximators, *Neural Netw* **2**(5):359–366, 1989.
22. Press WH *et al.*, *Numerical Recipes in C++: The Art of Scientific Computing* Cambridge University Press, 2002.
23. Bishop C, *Neural Networks for Pattern Recognition*, Oxford University Press, 1995.
24. López R, An open source neural networks C++ library. OpenNN, Intelnics (2013), Available at (www.intelnics.com/opennn).